

Eigenfrequency Analysis of a Helical Spring Electrode

Pratheev Sreetharan

December 16, 2008

1 Physical Motivation

In the field of soft microrobotics, actuation is a key limiting component. Small, compliant actuators tend to have unfavorable characteristics in terms of bandwidth, range of motion, and energy delivery. An actuation concept, known as ‘electrochemical actuation,’ has the potential to overcome several of these limitations. In this concept, an electrochemical cell is created in which one half-reaction results in a liquid-gas phase change. The gas pressure, when created in a compliant structure, can be used to produce useful actuation.

In one incarnation, a platinum wire wound into a helical spring is used as an electrode. The helix length is much longer than its diameter, and it is placed concentrically in a cylinder from which it must stay electrically isolated. One potential problem is that the phase change requires the creation of gas bubbles on the surface of this electrode. This issue is expected to become a serious problem as the scale of the actuator is reduced. To counter this problem, one proposal is to induce vibrations in the helical electrode through electromagnetic forces.

Resonant excitation is the most efficient technique to produce large bubble-dislodging velocities at the electrode surface. However, since the helix has low radial clearance with its cavity, only axial distortions are desired. It is necessary to define an electrode geometry with an ideal axial resonant mode far separated in frequency from undesired resonant modes. A finite element analysis has been undertaken to explore the resonant modes of an end-supported helix and how they vary with several available design parameters. The goal is to identify an electrode geometry with an isolated axial resonant mode at a useful frequency.

2 Finite Element Analysis

2.1 Software Package

The COMSOL Multiphysics simulation environment was used to undertake this analysis. The tool’s MATLAB interface allowed somewhat straightforward modelling of a complex three dimensional helical geometry without resorting to CAD modelling. The analysis was also rather fast, with meshing and analyzing taking less than 10 seconds on a reasonably capable machine.

2.2 Analysis Setup

A three dimensional helix was created and meshed in COMSOL. All surfaces were considered to be unconstrained except for the cross sectional surface at one end of the helix which was held fixed. Under these conditions, an undamped eigenfrequency analysis was conducted to identify the first 20 vibrational modes along with their frequencies.

The available design parameters of the helical electrode were taken to be the wire diameter d , the helix diameter D measured from the wire centerline, and the number of turns N . The nominal helix parameters were taken from an existing prototype with parameters $d = 0.5\text{mm}$, $D = 1.9\text{mm}$, and $N = 38$. Detailed helix parameters are given in §3.3.

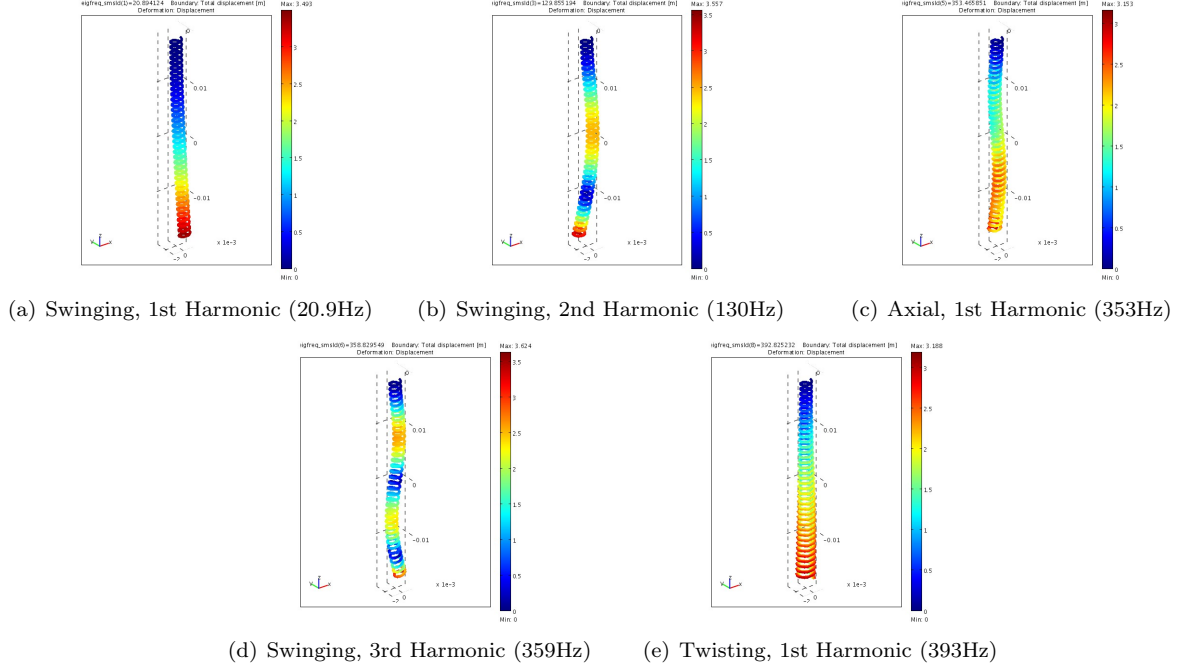


Figure 1: Normal modes are given in increasing frequency. The modes described in 1(a), 1(b), and 1(d) have a multiplicity of two corresponding to two independent directions of vibration. Frequencies are given for the nominal helix parameters.

2.3 Analysis Results

The results of analyzing the nominal helix are summarized in Figure 1. The lowest energy axial mode, shown in 1(c), is the desired vibrational mode, and in this configuration has a frequency of 353Hz. It is interesting to note the slight bending character of this axial vibrational mode. This is because the mode is separated from the 3rd harmonic of the swinging mode, shown in 1(d), by only 6Hz. The small separation has led to some degree of mixing between the two modes. This can be understood intuitively by realizing that if the frequencies were identical, then any linear combination of the two modes would also be an acceptable mode.

An unfortunate feature of having these poorly separated modes is that it will be difficult to excite the axial mode without injecting energy into the nearby swinging mode. This could compromise the performance of an actuator with a tight tolerance on radial displacement of the helical electrode.

To address this problem, the eigenfrequency analysis was run across various values of the number of turns N , the wire diameter d , and the helix diameter D . Plots of how the resonant frequencies change with each parameter are presented in Figures (3), (4), and (5), respectively.

Some rather interesting conclusions can be drawn from the results of this study. An examination of Figure (4) reveals that altering wire diameter does not affect the frequency separation between the desired axial normal mode from the nearby swinging normal modes. However, both the number of turns and the helix diameter can be altered in order to produce the desired frequency separation. This knowledge of which parameters can be used to increase mode frequency separation will inform subsequent electrode designs should radial vibrational displacement prove to be an issue.

The hypothesis that mode mixing was the reason for the existence of radial displacement in the predominantly axial normal mode was investigated by testing a helix geometry in which these modes were more separated. The radial displacement disappeared, confirming the conjecture. Supporting videos of this investigation are present in the related PowerPoint presentation.

Another interesting feature of this study is the sharp trend change for small helix diameters D in Figure (5). A theory to explain this change involves the pitch angle of the helix. The pitch angle α is a dimensionless parameter defined to be the angle between the helix wire and the plane perpendicular to the axis of the

helix. For large D , α is small and relatively constant. As D decreases, α begins to grow rapidly. The theory is that this rapid growth of pitch angle has a large effect on the resonant frequencies at small D , but not for larger D . This theory has not been tested.

It should be noted that while the bending and twisting vibrational modes of the helix are difficult to treat analytically, the axial modes lend themselves to a straightforward analysis. A comparison between theoretical and numerical results is useful, because agreement between both methods for these modes lends powerful support to the veracity of the numerical results for the analytically intractable modes. This comparison for the axial resonant modes follows.

3 Theoretical Derivation of Axial Normal Mode Frequencies

3.1 The Spring Constant

For an axial displacement, a helical coil can be approximated as an ideal massive spring. The axial displacement δ is proportional to the applied force P :

$$P = k\delta$$

The spring constant k is defined by the following expression [1]:

$$k = \frac{Gd^4}{8ND^3} \quad (1)$$

In (1), N is the number of turns, G is the shear modulus and d is the diameter of the wire. The quantity D is the winding diameter of the helix as traced by the center of the wire. The shear modulus G can be written in terms of Poisson's ration ν and Young's Modulus E :

$$G = \frac{E}{2(1 + \nu)}$$

Substituting into (1) gives:

$$k = \frac{Ed^4}{16(1 + \nu)ND^3} \quad (2)$$

3.2 Theoretical Axial Normal Mode Frequency

To calculate normal modes of a massive spring of length L , we can treat it as a one dimensional rod with modified geometric and material parameters. All relevant parameters of the rod, such as the Young's Modulus (E'), density (ρ'), cross sectional area (A'), will be denoted by primes. The effective Young's Modulus is:

$$E' = \frac{kL}{A'}$$

Using the tools of solid mechanics, the equation of motion for the displacement field $u(x)$ is:

$$\frac{\partial^2 u}{\partial t^2} = \left(\frac{E'}{\rho'}\right) \frac{\partial^2 u}{\partial x^2} = \left(\frac{kL}{\rho'A'}\right) \frac{\partial^2 u}{\partial x^2}$$

Note that the quantity $\rho'A'$ is the linear density ρ_l of the helical spring, which can be calculated from the helix geometry:

$$\rho_l = \frac{1}{4}\rho\pi d^2 \sqrt{1 + \pi^2 N^2 \left(\frac{D}{L}\right)^2}$$

Introducing the wave speed c allows:

$$c \equiv \sqrt{\frac{kL}{\rho_l}}$$

$$\frac{\partial^2 u}{\partial t^2} = c^2 \frac{\partial^2 u}{\partial x^2}$$

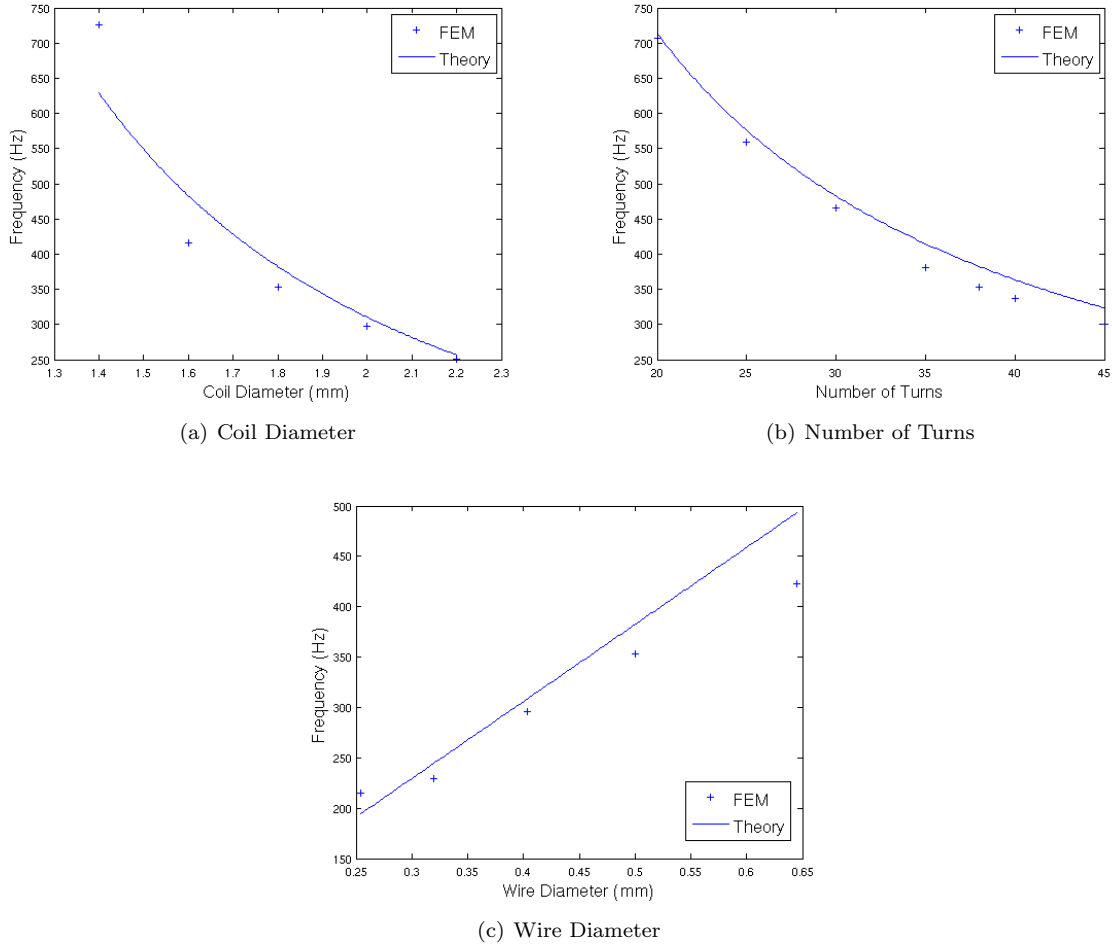


Figure 2: For the axial vibration normal mode, theoretical calculations from §3.2 are plotted against the results from finite element modeling. The lowest energy $n = 0$ mode from Figure 1(c) is shown.

Using the boundary conditions of one fixed end and one free end, calculation of the normal mode frequencies of axial oscillation is straightforward. The frequency of oscillation of the n^{th} normal mode, f_n , is:

$$\begin{aligned}
 f_n &= \frac{c}{2L} \left(\frac{1}{2} + n \right) \\
 &= \sqrt{\frac{k}{4L\rho_l}} \left(\frac{1}{2} + n \right)
 \end{aligned}$$

All quantities in this equation are now known. Platinum wire was used in all trials. From COMSOL's material database, we have the Young's Modulus $E = 168\text{GPa}$, the Poisson's Ratio $\nu = 0.38$ and the density $\rho = 2.145 \times 10^4 \frac{\text{kg}}{\text{m}^3}$.

3.3 Agreement with Numerical Analysis

For the nominal electrode, we have the following parameters¹:

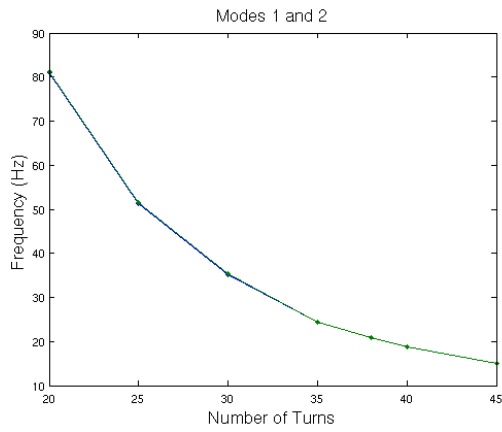
$$\begin{aligned}d &= 0.5\text{mm} \\D &= 1.8\text{mm} \\N &= 38 \\L &= 36.1\text{mm}\end{aligned}$$

These parameters result in a theoretical eigenfrequency $f_0 = 382\text{Hz}$, to be compared with the finite element result of $f_0 = 353\text{Hz}$, an error of 7.6%. Across all parameters of investigation, the theoretical axial mode frequency was comparable with the numerical one. Plots of numerical data vs theoretical data are shown in Figure 2. The close correlation between numerical and theoretical results lends credibility to the numerical results, and to the conclusions given in §2.3.

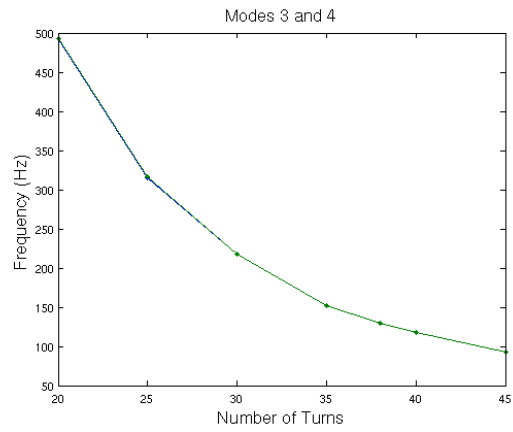
References

- [1] Budynas, Richard G., Charles R. Mischke, and Joseph E. Shigley. MECHANICAL ENGINEERING DESIGN. McGraw-Hill Professional, 2003.
- [2] Hibbeler, R. C. MECHANICS OF MATERIALS. Pearson Prentice Hall, NJ, 2005.

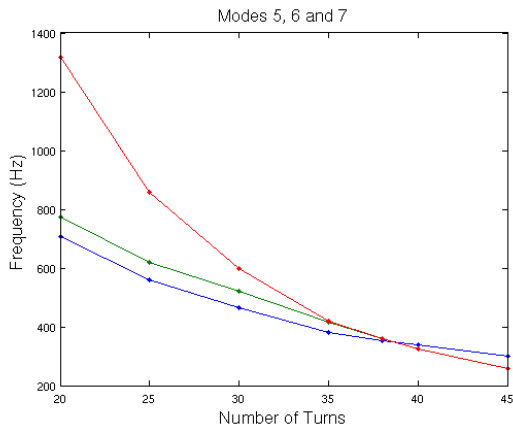
¹There is an inconsistency in the PowerPoint presentation given in class. Though the results presented are accurate, there are typographical errors in the reported nominal L and D . The values given in this paper are correct.



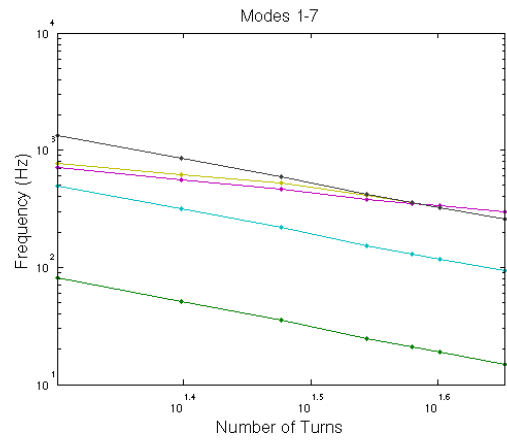
(a) Modes 1 and 2



(b) Modes 3 and 4

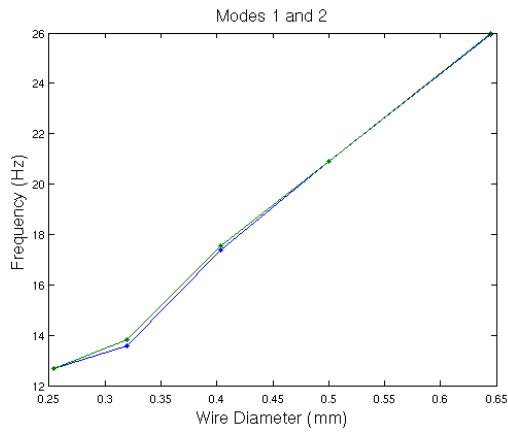


(c) Modes 5, 6, and 7

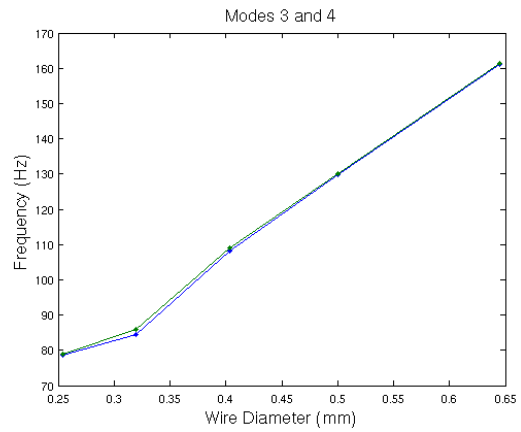


(d) Log Plot, Modes 1-7

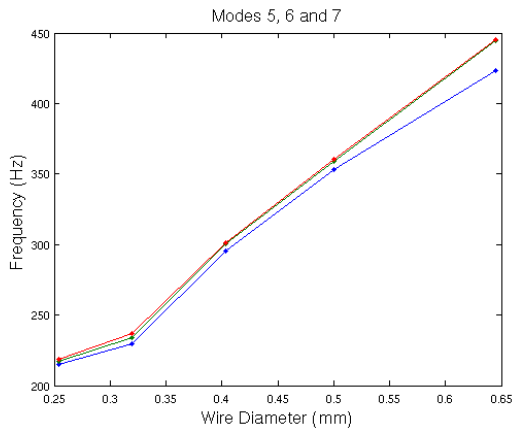
Figure 3: Dependence of vibrational mode frequencies on number of helical turns N , under a constant pitch angle. Increasing turn number decreases spring stiffness, lowering all resonant frequencies. The desired axial mode is mode 5, plotted in red in 3(c). Decreasing N is a good way to achieve separation between this mode and others.



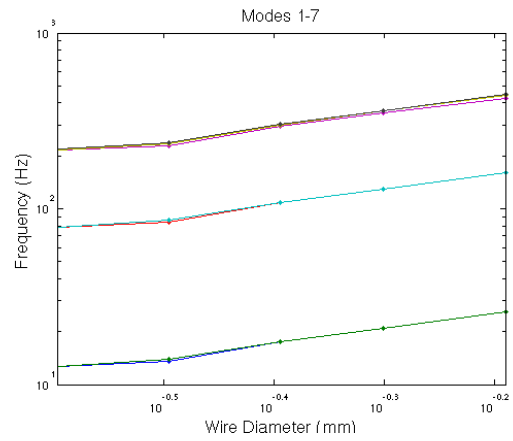
(a) Modes 1 and 2



(b) Modes 3 and 4



(c) Modes 5, 6, and 7



(d) Log Plot, Modes 1-7

Figure 4: Dependence of vibrational mode frequencies on wire diameter d . Increasing d increases spring stiffness, increasing all resonant frequencies. The desired axial mode is mode 5, plotted in red in 4(c). Modes 5, 6, and 7 all appear to have an equivalent dependence on d , so the wire thickness cannot be used to separate the resonant frequencies of these modes.

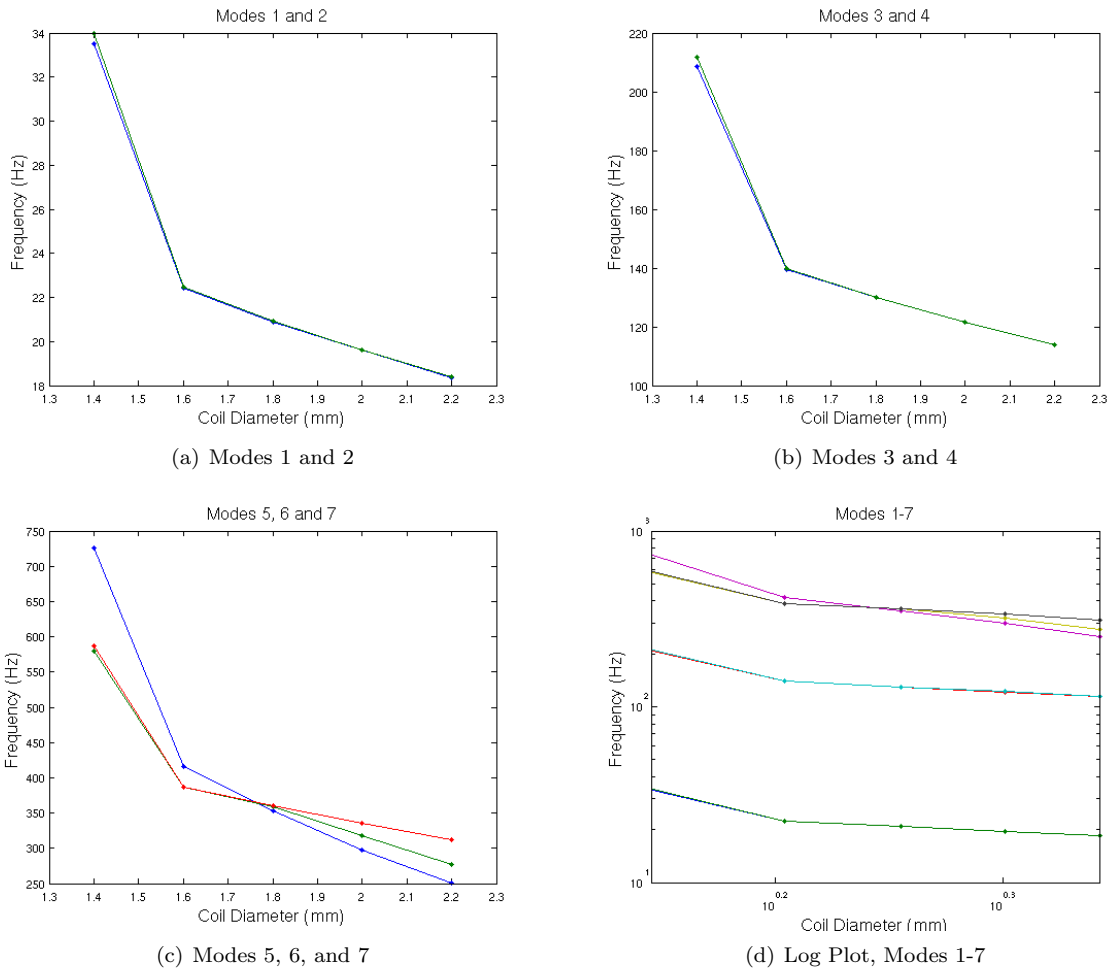


Figure 5: Dependence of vibrational mode frequencies on coil diameter D . Increasing d decreases spring stiffness, decreasing all resonant frequencies. The desired axial mode is mode 5, plotted in blue in 5(c). Modes 5, has a different dependence on D than do the swinging modes 6 and 7, so altering D of the helical coil can separate this desired mode from the two others nearby.